*Complex Systems Stability & Control*
https://www.sciltp.com/journals/cssc



*Article*

# Modeling Following Behavior Using Driver Memory and Leader's Optimal Speed

Limei Liu *, Xia Li and Yang Chen

School of Preparatory Education, Yunnan Nationalities University, Kunming 650500, China
* Correspondence: limei0329@139.com

**How To Cite:** Liu, L.; Li, X.; Chen, Y. Modeling Following Behavior Using Driver Memory and Leader's Optimal Speed. *Complex Systems Stability & Control* **2026**, *2*(4), 4. https://doi.org/10.53941/cssc.2026.100027

Received: 5 May 2026
Revised: 7 July 2026
Accepted: 14 August 2026
Published: 20 October 2026

**Abstract:** This work proposes an innovative car-following model that incorporates driver's sensory memory and the preceding vehicle's optimal velocity within the framework of the full velocity difference (FVD) model. First, the traffic stability criterion is calculated through the use of the theory of linear stability. Using a reductive perturbation technique, we construct the mKdV (modified Korteweg-de Vries) equation. Second, as the system approaches the critical point, the soliton of kink-antikink type obtained from the mKdV equation describes the traveling-wave behavior of jammed traffic. An analysis is also performed on the congestion magnitude and the energy expended. Finally, computational modeling is used to validate the theoretical findings, and the results show that the revised model is useful. According to numerical experiments and analytical derivations, the proposed model increases the optimal velocity coefficient, reduces memory requirements, mitigates traffic jam, strengthens traffic flow stability, and reduces kinetic energy fluctuations.

**Keywords:** FVD model; driver's sensory memory; mKdV equation; numerical simulations

## 1. Introduction

In light of continuous socioeconomic growth and the acceleration of modern city growth, the quantity of motor vehicles on the road has increased rapidly in recent decades, which leads to serious traffic problems, including road bottlenecks, vehicle collisions, environmental pollution [1–3]. Researchers have established numerous traffic flow models by studying the internal mechanisms and principles of the traffic system to alleviate traffic problems. These models, such as cellular automata models [4–6], hydrodynamic lattice models [7–9], continuum models [10–12], car-following models [13–17], are used to analyze and describe complex traffic phenomena from different perspectives and then reduce traffic congestion.

One essential type of model at the microscopic level is the car-following framework with strong practical application background due to its ability to easily capture real-time traffic dynamics, such as oscillatory traffic behavior and congestion growth [17]. Considering the influence of front and rear vehicle speeds, Pipes [18] devised a relative velocity-acceleration car-following model in a single lane. Considering that the vehicle's velocity was affected by the headway, Newell [19] developed a car-following model including the optimal velocity function in the early stages. In 1995, Bando et al. [20] derived a widely used optimal velocity (OV) model, which effectively described the evolutionary behavior characteristics of traffic congestion changes in a straightforward manner. On the basis of the OV model, researchers have proposed various improved models of car-following behavior that account for additional elements. To eliminate the shortcomings of the OV model in simulating excessively high acceleration and impractical braking behavior, the negative impact of speed differences is taken into account. So, Helbing et al. [21] integrated it into the OV framework and obtained the generalized force (GF) model. After that, Jiang et al. [22] modified it and incorporated the positive velocity difference to obtain the currently widely used

**Copyright:** © 2026 by the authors. This is an open access article under the terms and conditions of the Creative Commons Attribution (CC BY) license (https://creativecommons.org/licenses/by/4.0/).
**Publisher's Note**: Scilight stays neutral with regard to jurisdictional claims in published maps and institutional affiliations.

full velocity difference (FVD) model. Ge et al. [23] constructed the two-velocity-difference (TVD) strategy relying on a smart prompt structure. Since vehicle following is inherently a dynamic process, the operational state of the leading vehicle in the preceding few seconds tends to propagate to the following vehicle in the next moment. Hence, the information of the leading vehicle is the primary factor influencing the current vehicle's motion. So, Peng et al. [24] developed a model called optimal velocity difference (OVD) framework. Subsequently, many factors affecting traffic flow were included in the models [25–28]. These models are obviously helpful in improving the stabilization of traffic conditions.

The following analysis focuses on stability and sensitivity, conservation laws and exact solutions of fractional-order nonlinear equations, modulation instability of generalized nonlinear wave equations, as well as related studies on soliton structures and nonlinear wave propagation [29–31]. Regarding car-following models, some scholars have conducted research on car-following models using bifurcation analysis [32,33]. Moreover, a fractional-order car-following model has also been proposed [15]. However, for the research on car-following models, the most commonly used method at present is to solve them using the nonlinear stability analysis method that combines linear stability analysis and the reductive perturbation method [34–36].

Having analyzed the above models and recognized the complexity of actual traffic flow, we conclude that drivers have to consider various aspects throughout the driving process to ensure vehicle safety. The driving information of the leading car should be taken into account in order to achieve optimal operation conditions of the vehicle in actual traffic. However, the following vehicle's driver relies on past information and consequently requires a certain time to respond to the motion status of the leader [31]. Therefore, this period should be avoided to the greatest extent possible. Moreover, previous models either relied solely on the influence of speed memory or only considered one type of influence, such as distance memory. This paper considers the influence of both speed memory and distance memory. Considering the above situation, the contribution of the current driver's memory and the ideal velocity of the leading automobile is considered in traffic flow based on the FVD model.

In Section 2, we presents the extended framework, which includes the leading vehicle's optimal velocity as well as the current driver's memory effect. The stability of the model is examined in Section 3. In Section 4, we derives the mKdV equation by solving the model equation via the perturbation reduction approach for analyzing nonlinear systems. In Section 5, we carry out virtual experiments. In Section 6, we summarize and analyze the conclusions.

## 2. Model Formulation

In 1995, Bando et al. [20] derived a widely used optimal velocity (OV) model, and it effectively described the changing behavior characteristics of traffic congestion changes. The equation that describes the model is:

$$\frac{dv_n(t)}{dt} = a[V(\Delta x_n(t)) - v_n(t)], \tag{1}$$

where $x_n(t)$, $v_n(t)$, $\Delta x_n(t)$ and $a$ are displayed in Table 1. $V(\Delta x_n(t))$ refers to the headway-dependent optimal velocity, and it is written as [20]:

$$V(\Delta x_n(t)) = \frac{v_{\max}}{2}[\tanh(\Delta x_n(t) - h_c) + \tanh(h_c)], \tag{2}$$

here, $v_{\max} = 2$ and $h_c = 4$ are displayed in Table 1.

Based on the OV model, plenty of improved traffic flow models with additional factors were proposed. The aim is to overcome the OV model's disadvantages, specifically its excessive acceleration and unrealistic deceleration. Jiang et al. [22] modified it and offered a full velocity difference (FVD) prototype is a car-following model that is more widely used and more practical than the OV framework. It is presented as:

$$\frac{dv_n(t)}{dt} = a[V(\Delta x_n(t)) - v_n(t)] + \lambda[v_{n+1}(t) - v_n(t)], \tag{3}$$

$v_{n+1}(t) - v_n(t)$ and $\lambda$ are listed in Table 1.

In fact, because the driving of the vehicles is a dynamic following phenomenon of change, the behavior of the front vehicle in the first several seconds often turns into that of the trailing vehicle at the subsequent moment. Therefore, the most important factors affecting the current vehicle running status are the information of the front car. The optimal velocity difference (OVD) framework is given by Peng [24]. The motion equation is given by:

$$\frac{dv_n(t)}{dt} = a[V(\Delta x_n(t)) - v_n(t)] + \lambda \Delta v_n(t) + \gamma[V(\Delta x_{n+1}(t)) - V(\Delta x_n(t))] \tag{4}$$

Similarly, we consider the OVD model to be in the following form:

$$\frac{dv_n(t)}{dt} = a\{V(\Delta x_n(t)) + \gamma[V(\Delta x_{n+1}(t)) - V(\Delta x_n(t))] - v_n(t)\} + \lambda \Delta v_n(t), \tag{5}$$

namely

$$\frac{dv_n(t)}{dt}=a\{\gamma \mathrm{V}(\Delta x_{n+1}(\mathrm{t}))+(1-\gamma)\mathrm{V}(\Delta x_n(\mathrm{t}))-v_n(t)\}+\lambda \Delta v_n(\mathrm{t}). \tag{6}$$

where $\gamma$ and $\mathrm{V}(\Delta x_{n+1}(\mathrm{t}))-\mathrm{V}(\Delta x_n(\mathrm{t}))$ are presented in Table 1.

**Table 1.** Summary of the parameters and variables.

| Symbols | Physical Meaning | Symbols | Physical Meaning |
|---|---|---|---|
| $x_n(t)$ | location of the $n$ th vehicle | $\tau$ | reciprocal of the delay time ($s$) |
| $v_n(t)$ | velocity of the $n$ th vehicle | $v_{\max}$ | maximum velocity: $v_{\max}=2$ |
| $\Delta x_n(t)$ | the gap separating vehicle $n+1$ from vehicle $n$ | $\gamma$ | coefficient of the optimal velocity |
| $a$ | sensitivity | $\mathrm{h_c}$ | safe distance for driving: $\mathrm{h_c}=4$ |
| $\mathrm{V}(\Delta x_{n+1}(\mathrm{t}))-\mathrm{V}(\Delta x_n(\mathrm{t}))$ | optimal velocity difference | $\tau_0$ | the current driver's headway changes with memory time ($s$) |
| $\tau_1$ | the current driver's memory time ($s$) of the velocity | $p$ | the driver's memory intensity, $0\le p\le 1$. |
| $\lambda$ | the coefficient | $\tau_m=p\tau_0$ | effective memory time (s), so $\tau_m\in[0,\tau_0]$ |
| $\mu$ | the speed difference parameter: $\mu=\xi/\tau$ | | |

In real traffic flow, drivers always keep past information in mind during driving. To capture the characteristics of the leading vehicle, following drivers need to spend time perceiving, understanding and predicting its driving conditions. Moreover, previous models either relied solely on the influence of speed memory or only considered one type of influence, such as distance memory. This paper simultaneously considers the influence of both speed and distance memory. Based on the FVD model, a traffic flow model considering the optimal velocity of preceding vehicles and the current driving memory has been established. The extended model formula is:

$$\frac{dv_n(t)}{dt}=a\{\gamma \mathrm{V}(\Delta x_{n+1}(\mathrm{t}))+(1-\gamma)\mathrm{V}[\frac{1}{\tau_0}\int_{t-\tau_0}^{t}\Delta x_n(\mathrm{s})\mathrm{ds}]-v_n(t)\}+\mu[v_{n+1}(t)-\frac{1}{\tau_1}\int_{t-\tau_1}^{t}v_n(\mathrm{s})\mathrm{ds})]. \tag{7}$$

$\tau_0$, $\tau_1$ and $\mu$ are summarized in Table 1

For convenience, the theoretical investigation and numerical solution of the model, let $\tau_1=\tau_0$, assuming that the driver has the same memory time for the headway and the velocity [2]. The equation reads:

$$\begin{aligned}\frac{dv_n(t)}{dt} &= a\{\gamma V(\Delta x_{n+1}(t))+(1-\gamma)V[\frac{1}{\tau_0}\int_{t-\tau_0}^{t}\Delta x_n(s)ds]-v_n(t)\}\\ &+\mu[v_{n+1}(t)-\frac{1}{\tau_0}\int_{t-\tau_0}^{t}v_n(s)ds]\end{aligned} \tag{8}$$

The discretization scheme can be written as [31]:

$$\begin{aligned}\frac{dv_n(t)}{dt} &= a\{\gamma V(\Delta x_{n+1}(t))+(1-\gamma)V[\frac{1}{m}\sum_{i=1}^{m}\Delta x_n(\mathrm{s_i})]-v_n(t)\}\\ &+\mu[v_{n+1}(t)-\frac{1}{m}\sum_{i=1}^{m}\Delta v_n(\mathrm{s_i})], s_i\in[t-\tau_0,t]\end{aligned} \tag{9}$$

By the mean value theorem for integrals, the averaged headway and velocity can be represented by their values at an effective memory delay $\tau_m\epsilon[0,\tau_0]$. Assuming that the driver has the same effective memory delay for both headway and velocity, we obtain

$$V(\frac{1}{\tau_0}\int_{t-\tau_0}^{t}\Delta x_n(s)ds)\approx V(\Delta x_n(t-\tau_m)),\ \frac{1}{\tau_0}\int_{t-\tau_0}^{t}v_n(s)ds\approx v_n(t-\tau_m). \tag{10}$$

Under this assumption, Equation (8) can also be expressed in the form below:

$$\begin{aligned}\frac{\mathrm{dv_n}(t)}{dt}=a\{\gamma \mathrm{V}(\Delta x_{n+1}(\mathrm{t}))+(1-\gamma)\mathrm{V}(\Delta x_n(t-\tau_m))-\frac{dx_n(t)}{dt}\}+\\ \mu[v_{n+1}(t)-v_n(t-\tau_m)]\end{aligned} \tag{11}$$

## 3. Small-Disturbance Stability Analysis

To investigate how the operator's memory and the leading vehicle's desired speed affect congestion suppression, the stability limit of model (11) is derived in this section via linear approximation. During the initial equilibrium period, drivers all maintained the optimal speed $V(h)$ determined by the prescribed safe distance $h$.

During the stable stage, the $n$-th vehicle follows this trajectory:

$$V(h)t = x_n^0(t) - hn, h = \frac{\mathrm{L}}{N}\ , \tag{12}$$

in which $N$ is the overall count of vehicles, $L$ represents the road length, $x_n^0(t)$ corresponds to the equilibrium location of vehicle $n$ at instant $t$. To find the linear stability criterion, suppose $y_n(t)$ represents the small disturbance relative to the steady-state driving. Then the position is as follows:

$$x_n(t) = x_n^0(t) + y_n(t), \tag{13}$$

introducing Equations (12) and (13) into Equation (11), the following is obtained

$$\begin{aligned}\frac{d^2y_n(t)}{dt^2} = a\left\{\gamma \mathrm{V}'(h)\Delta y_{n+1}(\mathrm{t}) + (1-\gamma)\mathrm{V}'(h)\Delta y_n(t-\tau_m) - \frac{dy_n(t)}{dt}\right\}\\ +\mu[\frac{dy_{n+1}(t)}{dt} - \frac{dy_n(t-\tau_m)}{dt}]\end{aligned}, \tag{14}$$

here $\mathrm{V}'(h)$ represents the rate of change of the desired speed, $\mu = \frac{\xi}{\tau}$.

Letting $y_n(t) = exp^{ink+zt}$ and let $\tau_m = p\tau$, Equation (14) is changed to the following form

$$z^2 = a[\mathrm{V}'(h)(e^{ik}-1)(\gamma e^{ik} + (1-\gamma)e^{-zp\tau}) - z] + \frac{\xi}{\tau}z(e^{ik} - e^{-zp\tau}), \tag{15}$$

and, $z = ikz_1 + i^2k^2z_2 + \cdots, e^{ik} = 1 + ik + \frac{1}{2}i^2k^2 + \frac{1}{6}i^3k^3\cdots$, the terms of $ik$ and $i^2k^2$ are:

$$\begin{aligned} z_1 &= V'(h),\\ z_2 &= \frac{V'(h)}{2}(1 + 2\gamma + 2\xi) + (V'(h))^2(\xi p\tau - (1-\gamma)p\tau - \tau).\end{aligned} \tag{16}$$

where $\tau = \frac{1}{a}$. If $z_2 > 0$, the resulting model is uniform and resilient to large-wavelength fluctuations, whereas the homogeneous flow is oscillatory when $z_2 < 0$. The traffic flow stable equilibrium is given:

$$a = \frac{2V\prime(h)(1+(1-\gamma)p-\xi p)}{1+2\gamma+2\xi}. \tag{17}$$

Consequently, the stability condition is expressed as follows:

$$a > \frac{2V\prime(h)(1+(1-\gamma)p-\xi p)}{1+2\gamma+2\xi}. \tag{18}$$

The neutral stability lines (solid) derived from linear stability analysis show the relationship connecting sensitivity factor and gap under varying choices of $\gamma$ and $p$ when $\xi = 0.1$, $\mathrm{h_c} = 4$ in Figure 1a,b. The coexisting curves illustrated in the dotted lines are derived from the subsequent nonlinear analysis. Above the stability threshold, traffic jams do not arise; instead, the traffic stream is in a steady state. As shown in Figure 1a, the control coefficients $\gamma = 0.3$ and $p = 0, 0.3, 0.6, 1$ respectively, it can be found that every curve possesses a critical point, and the neutral stability curves, coexisting curves and critical points rise gradually with the increase of parameter $p$.Traffic behavior is steady as driver's memory intensity $p$ diminishes.

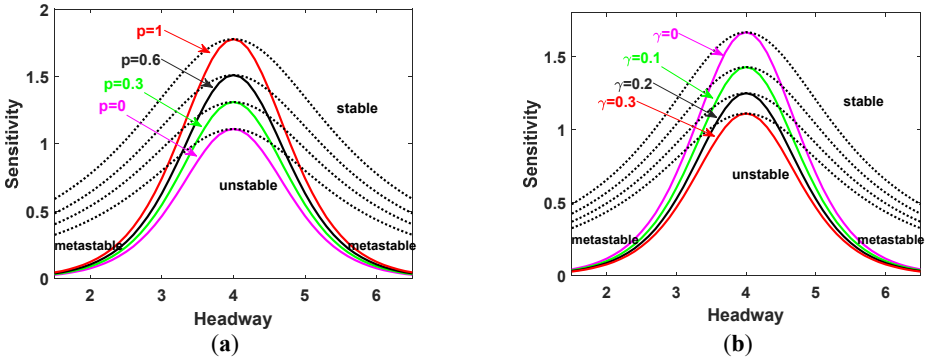



**Figure 1.** Presenting the neutral stability curves and coexistence curves: (**a**) for varying $p$ with $\gamma = 0.3$, and (**b**) for varying $\gamma$ with $p = 0$.

Therefore, a decrease in the driver's memory capacity has a positive effect on maintaining traffic stability. Let $p = 0$, take different values for $\gamma = 0, 0.1, 0.2, 0.3$. Then, we get different neutral stability curves, depicted in Figure 1b.As shown in Figure 1b, the results indicate that the stability region becomes progressively larger as $\gamma$ increases. This implies that increasing $\gamma$ leads to improved stability of traffic flow.

In addition, different influences of driver's memory intensitypand coefficient $\gamma$ in headway-sensitivity space $(\Delta x, a)$ are also discussed from Figure 2. Let's make $p = 0$ and $\gamma = 0$ the so-called FVD framework, and let's make $p = 0$ and $\gamma = 0.2$ that is OVD formulation. It can be seen from Figure 2 that the OVD scheme offers broader stability regions compared to the FVD one. In actual traffic, drivers will inevitably stay in the past memory. The stable region of driver's sensory memory intensity $p = 0.3$ OVD model still surpassed that the corresponding value of FVD model without memory influence. Given the importance of the optimal velocity of the leading vehicle in improving traffic stability. Therefore, one finds that $\gamma$ of the optimal velocity for leading vehicle supports the stabilization of traffic flow.

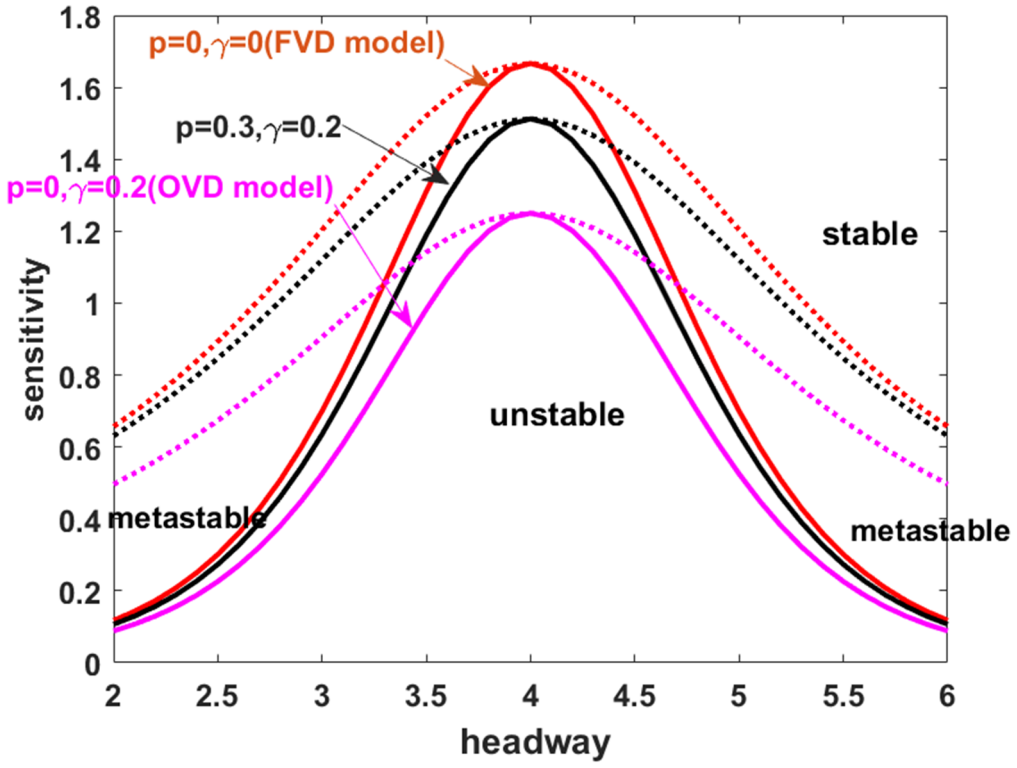



**Figure 2.** State diagram in the headway–sensitivity plane $(\Delta x, a)$ for various values of p and $\gamma$ at $\lambda = 0.1$ and $h_c = 4$.

## 4. mKdV Equation

To study the way density waves propagate through traffic streams during traffic congestion, this section derives the mKdV equation for sluggish variation characteristic of model Equation (11) near $(h_c, a_c)$.As a matter of convenience, first convert Equation (11) into the following structure:

$$\frac{d^2\Delta x_n(t)}{dt^2} = a\{\gamma[V(\Delta x_{n+2}(t)) - V(\Delta x_{n+1}(t))] + (1-\gamma)[V(\Delta x_{n+1}(t-\tau_m)) - V(\Delta x_n(t-\tau_m))] - \frac{d\Delta x_n(t)}{dt}\} + \mu[\frac{d\Delta x_{n+1}(t)}{dt} - \Delta v_n(t-\tau_m)], \quad (19)$$

Given $\varepsilon$ $(0 < \varepsilon \ll 1)$, the long-scale quantities $X, T$ are introduced and described next

$$X = \varepsilon(n + bt), T = \varepsilon^3 t, \quad (20)$$

b is the number to be determined. Then let the headway be in the following form:

$$\Delta x_n(t) = h_c + \varepsilon R(X, T), \quad (21)$$

Adopting Equations (20) and (21) within Equation (19), performing the fifth order of $\mathcal{E}$, one gives

$$\varepsilon^2 f_1 \frac{\partial R}{\partial X} + \varepsilon^3 f_2 \frac{\partial^2 R}{\partial X^2} + \varepsilon^4 (\frac{\partial R}{\partial T} - f_3 \frac{\partial^3 R}{\partial X^3} - f_4 \frac{\partial R^3}{\partial X}) + \varepsilon^5 (f_5 \frac{\partial^2 R}{\partial X \partial T} - f_6 \frac{\partial^4 R}{\partial X^4} - f_7 \frac{\partial^2 R^3}{\partial X^2}) = 0, \quad (22)$$

where: $f_1 = b - V', f_2 = b^2\tau - \gamma V' - \frac{1}{2}V' + bV'(1-\gamma)\tau_m - \lambda b(1 + b\tau_m), f_3 = \frac{1+6\gamma}{6}V' + \frac{1}{2}bV'\tau_m(1-\gamma)(\tau_m b - 1) + \frac{1}{2}\lambda b(1-(b\tau_m)^2)$ , $f_4 = \frac{1}{6}V''', f_5 = 2b\tau + V'(1-\gamma)\tau_m - \lambda(1+2b\tau_m), f_6 = \frac{1+14\gamma}{24}V' + (1-\gamma)V'(\frac{1}{4}(b\tau_m)^2 - \frac{1}{6}(b\tau_m)^3 - \frac{1}{6}b\tau_m) + \frac{1}{6}\lambda b(1+(b\tau_m)^3), f_7 = \frac{1}{6}V'''[\frac{1}{2} + \gamma - (1-\gamma)\tau_m b]$ and $V'(h_c) = \frac{dV(\Delta x_n)}{d\Delta x_n}|_{\Delta x_n(t)=h_c}, V'''(h_c) = \frac{d^3V(\Delta x_n)}{d\Delta {x_n}^3}|_{\Delta x_n(t)=h_c}$.

The mKdV equation is derived for study the slowly evolving behavior of the lengthy wave near $(h_c, a_c)$. To examine the development of the traffic congestion close to the critical point, setting $a_c/a = 1 + \varepsilon^2, b = V'$ and $\tau_m = p\tau$, into Equation (22) eliminating the coefficient of the terms $\varepsilon^2$ and $\varepsilon^3$, then get

$$\varepsilon^4 (\frac{\partial R}{\partial T} - h_1 \frac{\partial^3 R}{\partial X^3} + h_2 \frac{\partial R^3}{\partial X}) + \varepsilon^5 (h_3 \frac{\partial^2 R}{\partial X^2} + h_4 \frac{\partial^4 R}{\partial X^4} + h_5 \frac{\partial^2 R^3}{\partial X^2}) = 0, \quad (23)$$

where, $h_1 = \frac{1+6\gamma}{6}V' + \frac{1}{2}(1-\gamma)V'^2 p\tau_c(p\tau_c V' - 1) + \frac{1}{2}\lambda V'(1-(V'p\tau_c)^2), h_2 = -\frac{1}{6}V''', h_3 = V'(\frac{1+2\gamma}{2} + \lambda)$, $h_4 = [2\tau_c V' + (1-\gamma)p\tau_c V' - \lambda(1+2V'p\tau_c)][\frac{1+6\gamma}{6}V' + \frac{(1-\gamma)p\tau_c}{2}V'^2(V'p\tau_c - 1) + \frac{1}{2}\lambda V'(1-(V'p\tau_c)^2)] - \frac{1+14\gamma}{24}V' - (1-\gamma)V'(\frac{1}{4}(V'p\tau_c)^2 - \frac{1}{6}(V'p\tau_c)^3 - \frac{1}{6}V'p\tau_c) - \frac{1}{6}V'\lambda(1+(V'p\tau_c)^3)$ , $h_5 = \frac{V'''}{6}[2V'\tau_c + 2(1-\gamma)p\tau_c V' - \frac{1+2\gamma}{2} - \lambda(1+2V'p\tau_c)]$.

To obtain the normalized form, we perform the subsequent operations on Equation (23)

$$T' = h_1 T, R = \sqrt{h_1/h_2}R'. \quad (24)$$

Then substitute the Equation (24) formula into the Equation (23) formula,

$$\frac{\partial R'}{\partial T'} - \frac{\partial^3 R'}{\partial X^3} + \frac{\partial R'^3}{\partial X} + \varepsilon[\frac{h_3}{h_1}\frac{\partial^2 R'}{\partial X^2} + \frac{h_4}{h_1}\frac{\partial^4 R'}{\partial X^4} + \frac{h_5}{h_2}\frac{\partial^2 R'^3}{\partial X^2}] = 0, \quad (25)$$

letting $O[\varepsilon] = \varepsilon(\frac{h_3}{h_1}\frac{\partial^2 R'}{\partial X^2} + \frac{h_4}{h_1}\frac{\partial^4 R'}{\partial X^4} + \frac{h_5}{h_2}\frac{\partial^2 R'^3}{\partial X^2})$, ignore the $O(\varepsilon)$ expression in Equation (25). Therefore, the result is

$$R_0'(X,T') = \sqrt{C}\tanh[\sqrt{\frac{C}{2}}(X - CT')]. \quad (26)$$

To find the magnitude of the wave velocity $C$, the compatibility conditions are required to be fulfilled as below,

$$(R_0', M[R_0']) = \int_{-\infty}^{+\infty} dX\, R_0'(X,T') M[R_0'(X,T')] = 0, \quad (27)$$

here, $M[R_0'] = M[R']$.

After, we give the traveling speed $C$ as

$$C = \frac{5h_2h_3}{2h_2h_4 - 3h_1h_5}. \quad (28)$$

Therefore, the anti-symmetric solitary wave associated with the distance gap in the modified KdV equation is expressed as

$$\Delta x_n(t) = h_c + \sqrt{\frac{h_1 C}{h_2}(\frac{\tau}{\tau_c} - 1)}\tanh\{\sqrt{\frac{C}{2}(\frac{\tau}{\tau_c} - 1)} \times [n + (1 - Ch_1(\frac{\tau}{\tau_c} - 1))t]\}. \quad (29)$$

Where $\tau_c$ critical delay time/memory time. The magnitude $A$ is

$$A = \sqrt{\frac{h_1 C}{h_2}(\frac{\tau}{\tau_c} - 1)}. \quad (30)$$

In the coexisting scenario, one finds a low-density free-moving region alongside an additional region, is described by the kink-antikink soliton solution of congestion at elevated density. The coexistence lines of the coexisting region is derived by $\Delta x = h_c \pm A$. Clearly, from Figure 1a,b that the phase areas are classified into stable parts, meta-stable regions and unstable regions. With the increase of $\gamma$, the neutral stability boundary and the coexisting branch descend, the corresponding value of critical stability point becomes smaller, which demonstrates that incorporating the optimal velocity of the leading car can increase traffic state stability . With the decrease of driver's memory intensity $p$, the critical stability point becomes smaller and coexisting curve become lower, traffic flow stabilizes further. Thus, it can be shown that consideration of OVD and driver's sensory memory positively impacts on traffic flow.

## 5. Numerical Simulations

Numerical simulations will be implemented to confirm the results of theoretical analysis.To facilitate numerical analysis, the headway and velocity memory terms of Equation (11) are Taylor expanded by ignoring the nonlinear terms, the expansion formula is thus:

$$\frac{dv_n(t)}{dt} = a\{\gamma \mathrm{V}(\Delta x_{n+1}(\mathrm{t})) + (1-\gamma)[\mathrm{V}(\Delta x_n(t)) - \tau_m \Delta v_n(t)\mathrm{V}'(\Delta x_n(t))] - v_n(t)\} + \mu[v_{n+1}(t) - v_n(t) + a_n(t)\tau_m], \tag{31}$$

Equation (31) is discretized by using the forward Euler finite difference scheme. The discretized form of Equation (31) is:

$$\mathrm{v_n(t+\Delta t) = v_n(t) + \Delta t a\{\gamma V(\Delta x_{n+1}(t)) + (1-\gamma)[V(\Delta x_n(t)) - \tau_m \Delta v_n(t) V'(\Delta x_n(t))] - v_n(t)\} + \Delta t \mu[v_{n+1}(t) - v_n(t) + a_n(t)\tau_m]}, \tag{32}$$

where

$$\mathrm{a_n(t) = \frac{1}{1-\mu\tau_m} a\{\gamma V(\Delta x_{n+1}(t)) + (1-\gamma)[V(\Delta x_n(t)) - \tau_m \Delta v_n(t) V'(\Delta x_n(t))] - v_n(t)\} + \mu \frac{1}{1-\mu\tau_m}[v_{n+1}(t) - v_n(t)]}, \tag{33}$$

and $\Delta x_n(\mathrm{t}+\Delta t) = \Delta x_n(\mathrm{t}) + \Delta t \Delta v_n(\mathrm{t}), \tau_m = p\tau$. The vehicle's speed is 0 in its initial state. We impose initial disturbance [13] in what follows,

$$\begin{cases} \Delta x_n(0) = \Delta x_n(1) = 4.0, n \neq N/2, N/2+1 \\ \Delta x_n(1) = 4.1, n = N/2, \\ \Delta x_n(1) = 3.9, n = N/2+1, \end{cases}, \tag{34}$$

where $N = 100$ represent the total number of vehicles, $L = 400$ is the total length of the road, every time step $\Delta t = 0.05$s. The headway of vehicle 1 is $\Delta x_N = x_1 - x_N$ and the leading vehicle of vehicle $N$ is vehicle 1. All vehicles are updated synchronously on the ring; no independent leading vehicle is imposed. Other default parameters are set as: $v_{\max} = 2$, $h_c = \frac{L}{N} = 4$, $a = 1.1$ and $\mu = 0.1$.

### *5.1. Headway Distribution*

Figure 3 illustrates the spatiotemporal evolution of the spacing after $t = 4850s$ under various values of $\gamma$. The coefficient $p = 0$ is fixed. Under normal traffic, the space-time plots for $\gamma = 0, 0.1, 0.2$ and $0.3$ are shown in Figure 3a–d. When $\gamma = 0, p = 0$, the model transforms into the FVD model. That is, the result in Figure 3a is the same as that in Reference [23]. As for parts in Figure 3a–c, it is evident that once small perturbations are superimposed on the homogeneous flow, the small deviations steadily amplify over time, and the system moves to a variable state, and the travel behavior became variable. At this time, a wavy congestion pattern traveling in the reverse direction arises, which is conclusion derived in the Section 3. With the increase of the coefficient $\gamma$, the amplitude of shock waves tends to stabilize, as traffic flow becomes increasingly stable, accompanied by a gradual easing of congestion. Then, in Figure 3d, when $\gamma = 0.3$, traffic congestion no longer occurs and the traffic conditions have become stable. Even under the influence of weak disturbance, the whole state enters the uniform flow state, because $a = 1.1$ satisfies the condition of Equation (18). Therefore, the optimal velocity of the car in front can improve the stability of the traffic flow process.

Figure 4 presents the headway patterns at $t = 4950$ s associated with Figure 3. Figure 4 shows results similar to those in Figure 3. It can be seen intuitively that with the coefficient increase of the quantity $\gamma$, the vehicle headway's fluctuation amplitude lessens progressively, indicating improved traffic stability.

Next, Figure 5 indicates the evolution in space and time of headway after $t = 4850\ s$ for different time of parameter $p = 1, 0.6, 0.3$ and $0, \gamma = 0.3$ is fixed, other parameters remain constant. Figure 5a show that, after a small perturbation is superimposed on the uniform flow, backward-propagating traffic congestion density waves emerge over time and become chaotic and highly unstable. This occurs because $a = 1.1$ lies outside the stability region; the resulting behavior is consistent with the solution of the modified KdV equation, and the traffic flow is governed by Equation (18). However, from patterns (a) to (d), when $p$ decreases, the height of the clustering wave in traffic diminishes and the driving behavior is gradually stable. Finally, in pattern (d), when $a = 1.1$, $\gamma = 0.3, p = 0$ is the value satisfying Equation (18), it always keeps a stable state even if small disturbance traffic flow is added to uniform flow. And let the result of Figure 5d with $p = 0$ and $\gamma = 0.3$ be compared with the result of the OVD model. With the decrease of drivers' memory intensity $p$, traffic congestion is relieved to a certain extent.

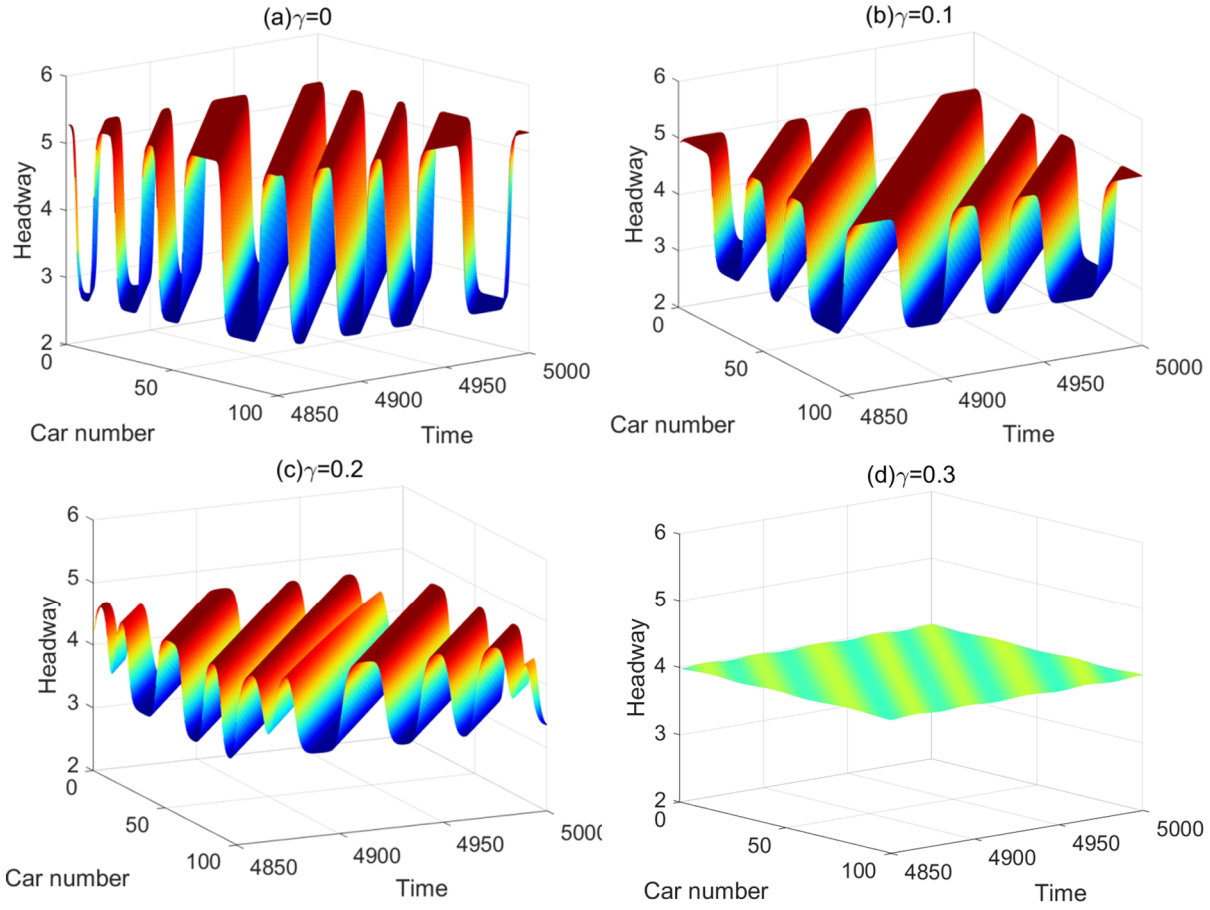



**Figure 3.** Space-time pattern of the inter-vehicle spacing after $t = 4850\ s$ for $p = 0$ and different values of $\gamma$.

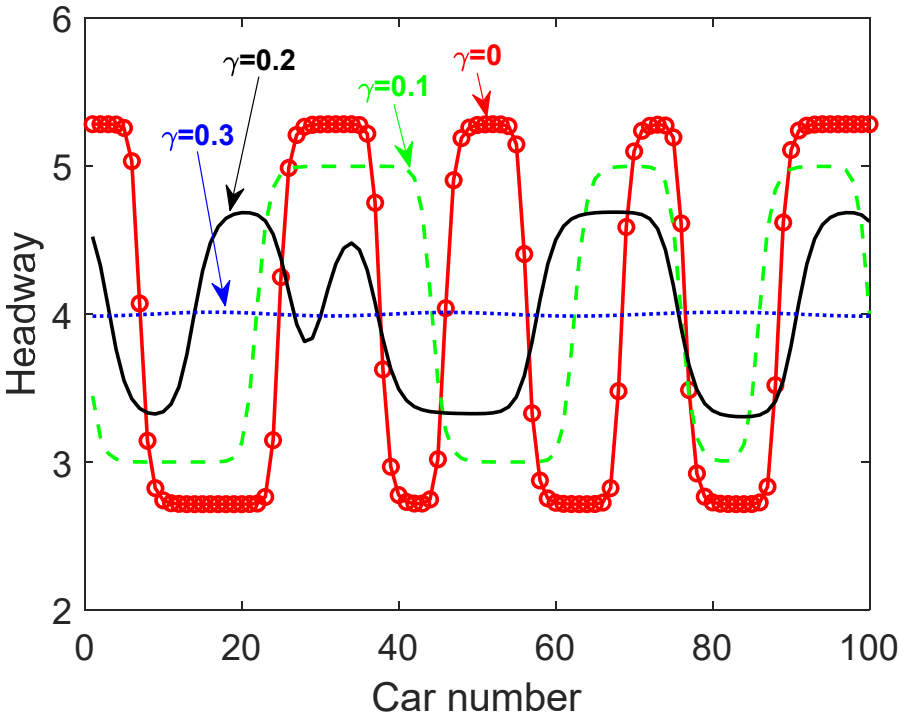



**Figure 4.** Headway patterns at $t = 4950\ s$ for different values of $\gamma$, corresponding to the cases in Figure 3.

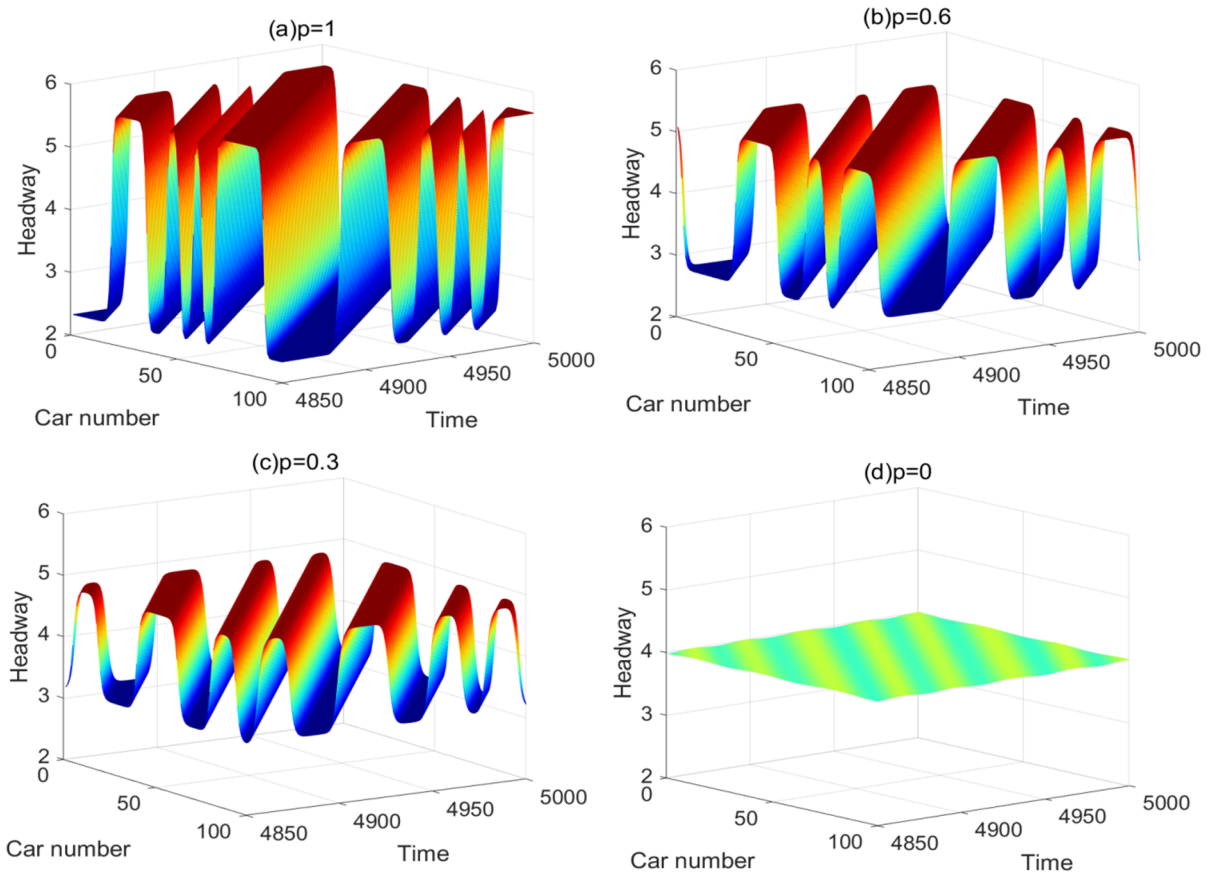



**Figure 5.** Space-time headway patterns after $t = 4850\ s$ for different values of p at $\gamma = 0.3$.

Figure 6 represents the spacing distributions at $t = 4950\ s$ associated with the patterns in Figure 5 respectively. Figure 6 gets the similar results of Figure 5. It can be seen intuitively that as the value of p decreases, the magnitude of vehicle spacing steadily shrinks, while driving behavior achieves a higher degree of stability. This aligns with the true nature of traffic.

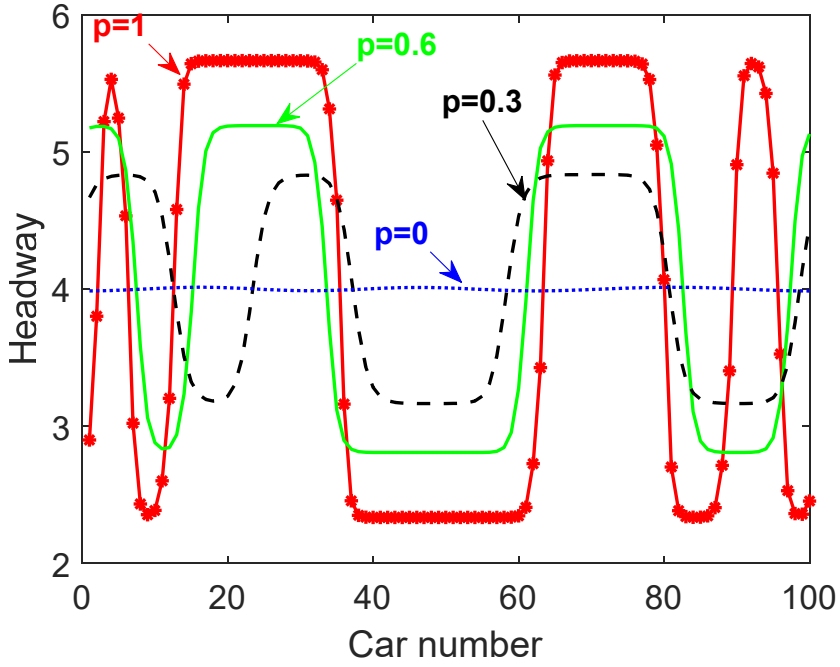



**Figure 6.** Headway profiles at $t = 4950\ s$ for different values of $p$, corresponding to the cases in Figure 5.

### *5.2. Hysteresis Loop*

In order to further study the role of the optimal velocity of the leading vehicle and current driver's memory on traffic flow, the hysteresis loop diagrams are drawn in Figure 7. Figure 7 shows the velocity-headway trajectory for different values of $\gamma$ and $p$. A smaller loop area leads to a smaller speed oscillations, and the traffic flow is more stable. It can be found in Figure 7a that with the progressive rise of $\gamma$, the hysteresis loop diagram area becomes smaller and traffic flow progressively stabilizes. Given that $p$ gradually decreases, the hysteresis loop area becomes smaller, and the vehicle flow remains steady in Figure 7b. Thus, the novel element exerts a beneficial impact on making traffic flow more stable.

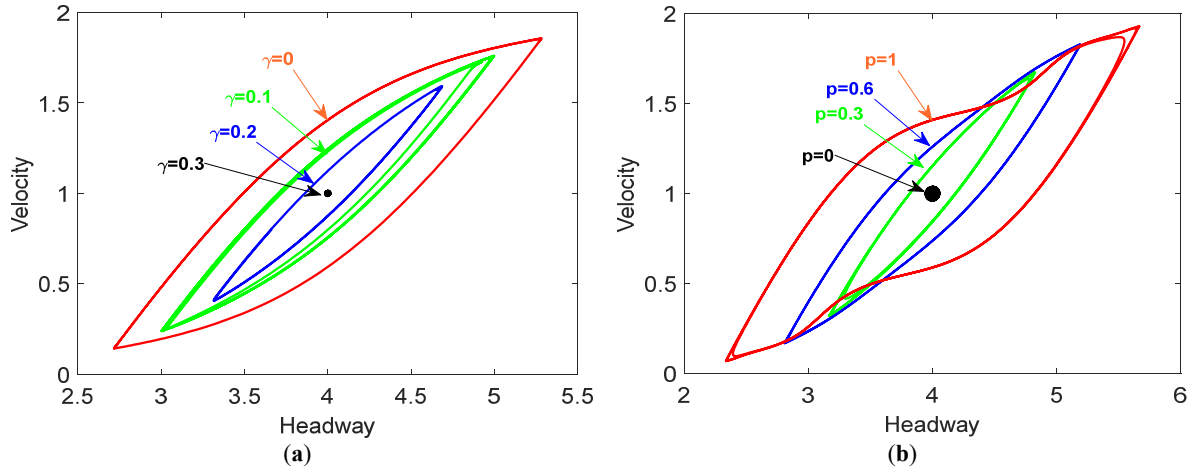



**Figure 7.** Hysteresis loops after $t = 4000\,s$ under different values: (**a**) parameter $\gamma$ $(p = 0)$, (**b**) parameter $p$ $(\gamma = 0.3)$.

### *5.3. Kinetic Energy Variation*

With ongoing urbanization and fast economic growth, the number of vehicles is growing at a much higher rate. In particular, traffic-induced energy consumption has remained a continual concern and has been the subject of study for many investigators. Under realistic traffic situations, the operations of traffic are influenced by multiple sophisticated conditions such as capability, the driver's personal characteristics, the information of the leading car and so on. Such influences perturb the steady driving behavior, leading to speed alterations that move through the stream like waves as time passes. Accordingly, these alterations in speed produce a higher level of energy expenditure [37–39].

The work-energy principle accounts for the energy expenditure of individual cars through the work they perform. Therefore, a thorough investigation of this principle enables a fine-grained quantification of the total energy consumption of road traffic [3]. Stated differently, to quantify the temporal variation of vehicular kinetic energy between two consecutive time instants, we define the instantaneous kinetic energy change as:

$$\Delta E_n = \frac{1}{2} m_n [v_n^2(k) - v_n^2(k-1)], \tag{10}$$

where $v_n(k)$,$v_n(k-1)$ are the car's speeds across two consecutive time intervals. To simplify the model, in this article we take $m = 1$.This quantity reflects the instantaneous rate of kinetic energy variation. A positive value $(\Delta E > 0)$ indicates that the vehicle is accelerating and its kinetic energy is increasing, while a negative value $(\Delta E < 0)$ corresponds to deceleration, where kinetic energy is being dissipated. The absolute magnitude of $\Delta E$ reflects the intensity of speed fluctuations.

From Figure 8a,b, two regions displaying with $\Delta E > 0$ and $\Delta E < 0$. When $\Delta E > 0$, the vehicle is accelerating (kinetic energy increases); when $\Delta E < 0$, it is decelerating (kinetic energy decreases). A smaller gap between the positive and negative peaks indicates smoother speed transitions and less abrupt acceleration/deceleration events. In Figure 8a, $p = 0.5$ , $a = 1.35$ and $\mu = 0.1$ are fixed and $\gamma$ is set to different values. With the increase of $\gamma$ value, kinetic energy variation gradually decreases and the gap between the energy expended in accelerating and braking gradually decreases. When $\gamma = 0.25$, kinetic energy variation approaches zero. In Figure 8b,$\gamma = 0.1$ is fixed and $p$ is set to different values. With the increase of $p$, the gap between speeding up and deceleration kinetic energy variation gradually increases, and kinetic energy variation gradually increases, which is in line with the actual situation.

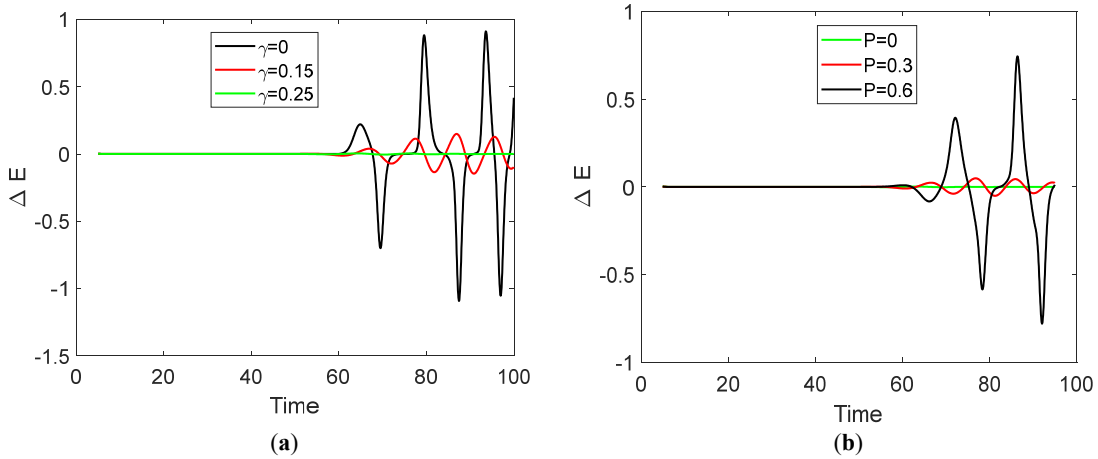



**Figure 8.** Profile of kinetic energy variation under different values: (**a**) parameter $\gamma$ ($p = 0.5$), (**b**) parameter $p$ ($\gamma = 0.1$).

## 6. Conclusions

Traffic bottleneck has a significant impact on people's everyday activities. A novel car-following model is proposed that incorporates both the driver memory and preceding vehicle's optimal velocity. Through the above investigation, it can be confirmed that increasing the coefficient$\gamma$of the leading vehicle's desired speed and reducing the memory intensity $p$ contribute to improved traffic flow stability.

Applying the linear stability method, we arrive at the constant-state conditions. The mKdV is deduced from nonlinear reduction perturbation technique to illustrate the dynamic qualities of the traffic jams near the critical unchanging point of phase diagram. Employing the solitary solution (kink-antikink) of the mKdV system, we also get the coexistence curves. These outcomes substantiate that the upgraded model can raise the level of stability in the traffic stream. The numerical simulations involve the evolution of spacing fluctuations, the plotting of hysteresis loops, and energy analysis. To ascertain the correctness of the speculative inferences, computer experiments are presented. The simulation conclusions show that the optimal velocity of the leading car can effectively suppress traffic jams. The effect of the current driver's short-term memory regarding traffic movement is consistent with actual driving situation. The results of numerical simulations agree with those of theoretical analysis. The paper analyzes the model using the nonlinear reductive perturbation method. This approach is relatively straightforward. Subsequently, the model will be analyzed from the perspective of bifurcation. Moreover, the model is limited to considering only the memory effect. Subsequently, we will introduce the jerk factor and road conditions to analyze the car-following model.

## Author Contributions

L.L.: conceptualization, methodology, formal analysis, validation, software, writing—original draft preparation, writing—review and editing; X.L.: validation, writing—review and editing; Y.C.: validation, writing—review and editing. All authors have read and agreed to the published version of the manuscript.

## Funding

This research received no external funding.

## Institutional Review Board Statement

Not applicable.

## Informed Consent Statement

Not applicable.

## Data Availability Statement

Data sharing is not applicable to this article as no datasets were generated or analyzed during the current study.

## Conflicts of Interest

The authors declare no conflict of interest.

## Use of AI and AI-Assisted Technologies

No AI tools were utilized for this paper.

## References


1. Cao, Z.; Jiang, S.; Zhang, J.; et al. A unified framework for vehicle rerouting and traffic light control to reduce traffic congestion. *IEEE Trans. Intell. Transp. Syst.* **2017**, *18*, 1958–1973. https://doi.org/10.1109/tits.2016.2613997.
2. Ma, G.; Ma, M.; Liang, S.; et al. Nonlinear analysis of the car-following model considering headway changes with memory and backward looking effect. *Phys. A* **2021**, *562*, 125303. https://doi.org/10.1016/j.physa.2020.125303.
3. Liu, L.; Li, W. Modeling and stability analysis of an extended car-following model behavior of the currents vehicle based on delay of response and signal interruption probability. *Proc. Inst. Mech. Eng. Part D J. Automob. Eng.* **2025**, *239*, 1355–1366. https://doi.org/10.1177/09544070231214829.
4. Moussa, N. Car accidents in cellular automata models for one-lane traffic flow. *Phys. Rev. E* **2003**, *68*, 036127. https://doi.org/10.1103/physreve.68.036127.
5. Wang, Z.; Chen, T.; Wang, Y.; et al. A cellular automaton model for mixed traffic flow considering the size of CAV platoon. *Phys. A* **2024**, *643*, 129822. https://doi.org/10.1016/j.physa.2024.129822.
6. Chen, T.; Wang, Z.; Xiang, J.; et al. Analysis of mixed traffic flow characteristics based on cellular automata model under lane management measures. *Phys. A* **2024**, *654*, 130177. https://doi.org/10.1016/j.physa.2024.130177.
7. Peng, G.; Liu, Y.; Tan, H.; et al. Phase transition in lattice hydrodynamic model integrating random anomalous information under connected autonomous vehicles surroundings. *Chaos Solitons Fractals* **2025**, *201*, 117274. https://doi.org/10.1016/j.chaos.2025.117274.
8. Liu, L.; Li, W.; Wang, X.; et al. Modeling and smooth driving feedback control for an extended lattice hydrodynamic model incorporating cyber-attacks. *Phys. Scr.* **2026**, *101*, 145212. https://doi.org/10.1088/1402-4896/ae5769.
9. Mehta, S.; Redhu, P.; Siwach, V. Stability analysis in multi-lane traffic flow model with density delay and lane-changing dynamics: A spatiotemporal and Lyapunov analysis. *Chaos Solitons Fractals* **2026**, *204*, 117793. https://doi.org/10.1016/j.chaos.2025.117793.
10. Jiang, R.; Wu, Q.S.; Zhu, Z.J. A new continuum model for traffic flow and numerical tests. *Transp. Res. B* **2002**, *36*, 405–419. https://doi.org/10.1016/s0191-2615(01)00010-8.
11. Jafaripournimchahi, A.; Cai, Y.F.; Wang, H.; et al. Stability analysis of delayed-feedback control effect in the continuum traffic flow of autonomous vehicles without V2I communication. *Phys. A* **2022**, *605*, 127975. https://doi.org/10.1016/j.physa.2022.127975.
12. Zhai, C.; Wu, W.; Xiao, Y.; et al. A novel throttle-based self-stabilizing control scheme integrated into an anisotropic continuum model to mitigate cyber-attacks in connected vehicle scenarios. *Chaos Solitons Fractals* **2025**, *201*, 117319. https://doi.org/10.1016/j.chaos.2025.117319.
13. Tang, T.Q.; Li, C.Y.; Huang, H.J. A new car-following model with the consideration of the driver's forecast effect. *Phys. Lett. A* **2010**, *374*, 3951–3956. https://doi.org/10.1016/j.physleta.2010.07.062.
14. Li, Z.; Qin, Q.; Li, W.; et al. Stabilization analysis and modified KdV equation of a car-following model with consideration of self-stabilizing control in historical traffic data. *Nonlinear Dyn.* **2018**, *91*, 1113–1125. https://doi.org/10.1007/s11071-017-3934-y.
15. Fu, Y.; Hu, W.; Shang, J.; et al. A fractional-order car-following model with random delay optimized by an enhanced whale optimization algorithm. *Nonlinear Dyn.* **2025**, *113*, 21277–21303. https://doi.org/10.1007/s11071-025-11271-4.
16. Tian, C.; Kang, Y. Modeling of flow-difference influences on dynamic phase transition and stability in curved road traffic systems. *Symmetry* **2025**, *17*, 1299. https://doi.org/10.3390/sym17081299.
17. Wu, Y.; Ma, Z.; Wang, Y.; et al. Nonlinear dynamics of traffic flow stability: A review from car-following to mixed-autonomy. *Chaos Solitons Fractals* **2026**, *208*, 118340. https://doi.org/10.1016/j.chaos.2026.118340.
18. Pipes, L.A. An operational analysis of traffic dynamics. *J. Appl. Phys.* **1953**, *24*, 274–281. https://doi.org/10.1063/1.1721265.
19. Newell, G.F. Nonlinear effects in the dynamics of car following. *Oper. Res.* **1961**, *9*, 209–229. https://doi.org/10.1287/opre.9.2.209.
20. Bando, M.; Hasebe, K.; Nakayama, A.; et al. Dynamical model of traffic congestion and numerical simulation. *Phys. Rev. E* **1995**, *51*, 1035–1042. https://doi.org/10.1103/physreve.51.1035.
21. Helbing, D.; Tilch, B. Generalized force model of traffic dynamics. *Phys. Rev. E* **1998**, *58*, 133–138. https://doi.org/10.1103/physreve.58.133.

22. Jiang, R.; Wu, Q.; Zhu, Z. Full velocity difference model for a car-following theory. *Phys. Rev. E* **2001**, *64*, 017101. https://doi.org/10.1103/physreve.64.017101.
23. Ge, H.X.; Cheng, R.J.; Li, Z.P. Two velocity difference model for a car following theory. *Phys. A* **2008**, *387*, 5239–5245. https://doi.org/10.1016/j.physa.2008.02.081.
24. Peng, G.H.; Cai, X.H.; Liu, C.Q.; et al. Optimal velocity difference model for a car-following theory. *Phys. Lett. A* **2011**, *375*, 3973–3977. https://doi.org/10.1016/j.physleta.2011.09.037.
25. Ma, G.; Li, K. Phase transitions of car following model considering driver characteristics and honk effect. *Chaos Solitons Fractals* **2025**, *201*, 117186. https://doi.org/10.1016/j.chaos.2025.117186.
26. Peng, G.; Li, X.; Wang, H.; et al. Bifurcation and phase transitions in car-following model integrating driver's characteristic and speed limit on spiral slope roads. *Chaos Solitons Fractals* **2024**, *186*, 115200. https://doi.org/10.1016/j.chaos.2024.115200.
27. Wang, W.J.; Ma, M.H.; Liang, S.D.; et al. Density waves in an improved car-following model under intelligent transportation system environment. *Mod. Phys. Lett. B* **2022**, *36*, 2250014. https://doi.org/10.1142/s0217984922500142.
28. Zhou, T.; Tian, Y.; Zhu, M.; et al. Phase transitions in mixed traffic streams comprising HDVs and CAVs through the implementation of delayed control mechanisms to mitigate traffic jerk. *Chaos Solitons Fractals* **2025**, *199*, 116679. https://doi.org/10.1016/j.chaos.2025.116679.
29. Shakeel, M.; Liu, X.G. Solitary wave solutions, bifurcation theory, and sensitivity analysis in the modified unstable nonlinear Schrödinger equation. *Mod. Phys. Lett. B* **2025**, *39*, 2550082. https://doi.org/10.1142/s0217984925500824.
30. Hosseini, K.; Hinçal, E.; Ilie, M. Bifurcation analysis, chaotic behaviours, sensitivity analysis, and soliton solutions of a generalized Schrödinger equation. *Nonlinear Dyn.* **2023**, *111*, 17455–17462. https://doi.org/10.1007/s11071-023-08759-2.
31. Cao, B.G. A new car-following model considering driver's sensory memory. *Phys. A* **2015**, *427*, 218–225. https://doi.org/10.1016/j.physa.2015.01.078.
32. Ai, W.H.; Lei, Z.Q.; Li, D.Y.; et al. Bifurcation analysis and control study of improved full-speed differential model in connected vehicle environment. *Chin. Phys. B* **2024**, *33*, 070503. https://doi.org/10.1088/1674-1056/ad3b80.
33. Guan, X.; Qin, J.; Cheng, R.; et al. Bifurcation and linear analysis of connected heterogeneous traffic flow model under cyberattacks. *Chaos Solitons Fractals* **2025**, *200*, 117018. https://doi.org/10.1016/j.chaos.2025.117018.
34. Wang, Y.J.; Song, H.; Cheng, R.J. TDGL and mKdV equations for an extended car-following model with the consideration of driver's memory. *Phys. A* **2019**, *515*, 440–449. https://doi.org/10.1016/j.physa.2018.09.171.
35. Sun, D.H.; Tan, P.; Chen, D.; et al. Burgers and mKdV equation for car-following model considering drivers' characteristics on a gradient highway. *Mod. Phys. Lett. B* **2018**, *32*, 1850314. https://doi.org/10.1142/s0217984918503141.
36. Yao, R.; Qiao, Y.; Xue, Y.; et al. Phase transitions and chaotic jam in multi-lane lattice hydrodynamic model considering driver anticipation and passing behavior. *Nonlinear Dyn.* **2026**, *114*, 398. https://doi.org/10.1007/s11071-026-12244-x.
37. Tang, T.Q.; Huang, H.J.; Shang, H.Y. Influences of the driver's bounded rationality on micro driving behavior, fuel consumption and emissions. *Transp. Res. Part D Transp. Environ.* **2015**, *41*, 423–432. https://doi.org/10.1016/j.trd.2015.10.016.
38. Xue, Y.; Kang, S.J.; Lu, W.Z.; et al. Energy dissipation of traffic flow at an on-ramp. *Phys. A* **2014**, *398*, 172–178. https://doi.org/10.1016/j.physa.2013.12.032.
39. Peng, G.H.; Lu, W.Z.; He, H.H. Nonlinear analysis of a new car-following model accounting for the global average optimal velocity difference. *Mod. Phys. Lett. B* **2016**, *30*, 1650327. https://doi.org/10.1142/s0217984916503279.